Precise Time-of-Flight Calculation For 3D Synthetic Aperture Focusing

Andresen, Henrik Stenby; Nikolov, Svetoslav; Jensen, Jørgen Arendt

Published in:
2007 IEEE Ultrasonics Symposium Proceedings

Link to article, DOI:
10.1109/ULTSYM.2007.67

Publication date:
2007

Document Version
Publisher's PDF, also known as Version of record

Precise Time-of-Flight Calculation For 3D Synthetic Aperture Focusing

Henrik Andresen[1,2], Svetoslav Ivanov Nikolov[1] and Jørgen Arendt Jensen[1]

1) Center for Fast Ultrasound Imaging, Ørsted•DTU,
Bldg. 348, Technical University of Denmark, DK-2800 Lyngby, Denmark.
2) B-K Medical, Mileparken 34, DK-2730 Herlev, Denmark.

Abstract— **Conventional linear arrays can be used for 3D ultrasound imaging, by moving the array in the elevation direction and stacking the planes in a volume. The point spread function (PSF) is larger in the elevation plane, as the aperture is smaller and has a fixed elevation focus. Resolution improvements in elevation can be achieved by applying synthetic aperture (SA) focusing to the beamformed in-plane RF-data. The method uses a virtual source (VS) placed at the elevation focus for post-beamforming. This has previously been done in two steps, in plane focusing followed by SA post-focusing in elevation, because of a lack of a simple expression for the exact time of flight (ToF). This paper presents a new method for calculating the ToF for a 3D case in a single step using a spherical defocused emission from a linear array. The method is evaluated using both simulated data obtained by Field II and phantom measurements using the RASMUS experimental scanner. For the simulation, scatterers were placed from 20 to 120 mm of depth. A point and a cyst phantom were scanned by translating a 7 MHz linear array in the elevation direction. For a point placed at $(25, 8, 75)$ mm relative to the transducer, the mean error between the calculated and estimated ToF is 0.0129 μs (0.09λ), and the standard deviation of the ToF error is 0.0049λ. SA focusing improves both contrast and resolution. For simulated scatterers at depths of 40 and 70 mm the FWHM is 83.6% and 46.8% of the FWHM without elevation SA focusing. The main-lobe to side-lobe energy ratio (MLSLR) for the scatterers is 32.3 dB and 29.1 dB. The measurement of a PSF phantom at a depth of 65 mm shows a relative FWHM of 27.8%. For an elevation sampling distance of 0.63 mm, the MLSLR for the two simulated scatterers is 26.4 dB and 27.9 dB. For the point phantom the MLSLR is 16.3 dB. If the elevation sampling distance is increased to 0.99 mm, the two simulated scatterers have a MLSLR of 21.1 dB and 15.8 dB respectively, and the point phantom has an MLSLR of 5.2 dB. The cyst phantom shows an improvement of 5.8 dB in contrast to noise ratio, for a 4 mm cyst, when elevation focusing is applied.**

I. Introduction

The use of linear array transducers to acquire 3D volume ultrasound (US) images is more common to 2D array acquisition. A linear array is readily commercially available, has relatively few elements and can be used with modern ultrasound scanners. A drawback is that the array must be mechanically moved for a volume acquisition, increasing acquisition time. 3D volume acquisition with linear arrays have traditionally been done by imaging one plane and moving the transducer, creating the 3D volume by stacking individual planes. These volumes have good lateral and depth resolution, but poor elevation resolution and contrast because of the small elevation aperture size.

Using synthetic aperture (SA) focusing technique to improve the resolution of a fixed focus transducer has been shown feasible in [1]. This has further been used in [2]–[4] with linear and phased array transducers, to allow for both lateral and elevation focusing. Here a set of planes are beamformed with SA focusing, generating a set of lateral scan-lines. The volume is created by beamforming the scan-lines in elevation by assuming that the elevation focus is a virtual source. Previous work has shown a significant increase in both elevation resolution, contrast, and signal to noise ratio (SNR) when applying this 2-step elevation beamforming method.

The method presented in this paper allows for a precise time of flight (ToF) calculation for lateral and elevation beamforming, using only a single beamforming step. This removes the requirement for beamforming in-plane points at the Nyquist criteria, and only uses points required for the volume. Section II will describe the equations and theory used in the method, the measurement setup is described in Section III, and Section IV will show the results from both simulation and measurements. The paper concludes in Section V.

II. Theory

SA focusing applied to linear arrays is traditionally done by calculating the ToF for a spherical wave emanating from a single point, allowing each emission to contribute to the focusing of the entire insonified region. As SA has an inherent low SNR, virtual sources (VS) [3], [5], [6] and frequency modulation [7] are used to increase the emitted energy.

The method of calculating the ToF is a two-fold process, as a VS is used both in the lateral and the elevation direction. The process is shown in Fig. 1 where the blue point is the desired beamformed point denoted $\vec{r}_p$, the red dotted lines show the acceptance angle for the transmit VS and the blue dashed lines show the acceptance angle for the VS placed at the elevation focus. The point $\vec{r}_p$ is projected onto the xz-plane (lateral - depth) by letting the depth of the point be the distance traveled by the sound on a plane orthogonal to the xz-plane, by placing a VS at the elevation focus on the same lateral position as $\vec{r}_p$. The depth of the new point will be given by

$$z_{\text{proj}} = \sqrt{r_{p,y}^2 + (r_{p,z} - z_{ele})^2} \cdot sign(r_{p,z} - z_{ele}) + z_{ele}, \quad (1)$$

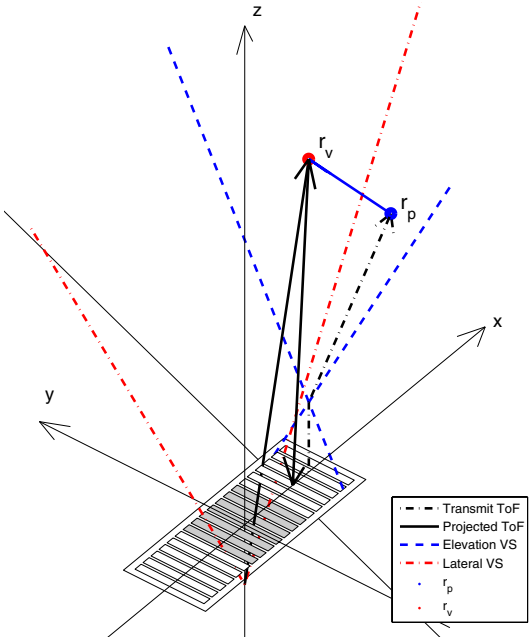

Fig. 1. Illustration of the ToF calculation. Red dotted lines are transmit VS acceptance angle, blue dashed lines are elevation focus acceptance angle, the dotted black line is transmit ToF for the beamformed point, and solid black line is the total ToF for the projectet point. The blue point $\vec{r}_p$ is the desired beamformed point, and the red point $\vec{r}_v$ is the virtual projected point.

where $r_{p,y}, r_{p,z}$ is the elevation and depth position of $\vec{r}_p$ relative to the transducer and z_{ele} is the depth of the elevation focus. This virtual point is used for the ToF calculation using in-plane SA focusing. The virtual point, denoted $\vec{r}_v$, will have the coordinates $(r_{p,x}, 0, z_{ele})$. The equation for the total ToF for a transmission to the m'th receive element is given by

$$t_{\text{ToF},m} = \frac{|\vec{r}_v - \vec{r}_{VS}| + |\vec{r}_v - \vec{r}_{rcv,m}|}{c}, \qquad (2)$$

where $\vec{r}_{VS}$ is the position of the transmit VS, $\vec{r}_{rcv,m}$ is the position of the m'th receiving element, and c is the speed of sound. The path is shown by the solid black line in Fig. 1.

The signal amplitude for a single point is given by summing the received signals at the time instances calculated by (2), which yields

$$s(\vec{r}_p) = \sum_{j=1}^{J} \sum_{m=1}^{M} \sum_{n=1}^{N} a_{j,m,n} \cdot g_{j,m,n}(t_{ToF,m}), \qquad (3)$$

where $a_{j,m,n}$ is the apodization and $g_{j,m,n}$ is the signal for the m'th receive channel, of the n'th emission at the j'th elevation position. M is the number of receive elements, N is the number of transmit VS's and J is the number of elevation positions.

III. Measurement Setup

All measurements were done with the RASMUS experimental scanner and a precision positioning system (called internally the xyz-system), both available at the Center for Fast Ultrasound imaging (CFU). RASMUS is an abbreviation for Remotely Accessible Software configurable Multi-channel Ultrasound Sampling system, and was designed as a very flexible US system capable of transmitting arbitrary waveforms and storage of raw single channel data. A more detailed description is found in [8]. The xyz-system allows for a precise movement of the transducer using a stepper motor with a step size of 5 μm. During the data acquisition the transducer is moved in steps of 0.09 mm, equal to 0.41 λ, in the elevation direction between each full scan-sequence. Pulse compression and filtration is attained with a matched filter created by time-inverting the emitted FM-chirp described in [7].

The transducer and in-plane scan sequence parameters are shown in Table I. The same scan sequence is used for simulation, and scanning of a single-PSF phantom and a cyst phantom. A total of 201 or 301 planes are acquired during a scan. After data acquisition, the data is beamformed off-line according to (3).

TABLE I
TRANSDUCER AND MEASUREMENT PARAMETERS.

Transducer type	Linear array
Number of transducer elements	64
Center frequency, f_0	7.0 MHz
Transducer element pitch	0.208
Transducer element height	4.5 mm
Elevation focus	25 mm
STA Scan Parameters	
Elements in virtual source	7
Emissions for full STA	64
Lateral VS Focusing F$^{\#}$	$-\frac{1}{2}$
FM-Chirp length	20 μs
Scan depth	80 mm
Receive apodization	Blackman
Receive F$^{\#}$	2
Elevation step-size	0.09 mm

IV. Results

To evaluate the methods ability to estimate an accurate ToF for an off-axis scatterer, a simulated pulse-echo response is compared to the value calculated by (2). All simulations uses Field II [9], [10] to calculate the pulse-echo response. Fig. 2 shows the envelope of the simulated pulse-echo response and the estimated ToF is shown by a solid black line. The estimated ToF is compared with the peak amplitude of the envelope detected simulated response. The difference in arrival time between the two has a bias of 0.09 λ, and the mean standard deviation is 0.0049 λ for a 7 MHz pulse. Compared to the conventional 2-step method for the same point, the bias is 0.12 λ, and the mean standard deviation is 0.0945 λ.

The methods ability to synthesize a larger aperture in elevation is evaluated from the full-width at half max (FWHM) and the main-lobe to side-lobe energy ratio (MLSL) of both simulated and measured scatterers. For a cyst phantom it is measured by the improvement of the contrast to noise ratio (CNR) in the lateral-depth plane. The CNR is calculated by the method given in [11].

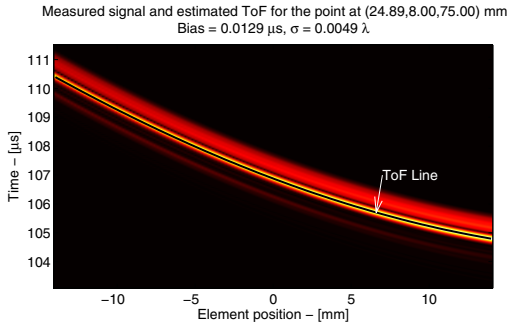

Fig. 2. Pulse-echo response from a single scatterer at position (25,8,75) mm relative to the transducer. The envelope of the RF-data is plotted at the receive channel position with the estimated ToF for each channel overlayed as a solid black line.

In Fig. 3, the FWHM for scatterers at 20 to 120 mm of depths is shown. With no elevation focusing a linear increase of the FWHM is seen as a function of depth. By applying 3D SA focusing, the constant $F^{\#}$ allows for a constant FWHM. The conventional 2-step focusing method show results similar to the 3D SA focusing, but has a slightly larger FWHM at deeper scatterers.

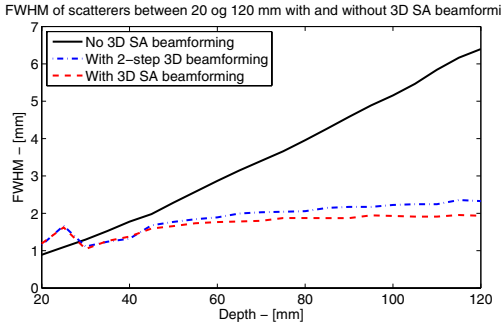

Fig. 3. Elevation FWHM for scatterers between 20 and 120 mm, with no, 2-step, and with 3D SA focusing.

For different elevation stepping sizes, the effect on a simulated scatterer at 70 mm of depth is shown in Fig. 4. For a stepping size of 0.09 mm the side-lobes are around -60 dB, while for 0.45 mm stepping size they are below -50 dB. An increase of the elevation step-size to 0.99 mm elevates the side-lobes to almost the same level as with no elevation focusing. The FWHM is unchanged by the stepping size, as the width of the synthesized aperture is the same. The values given in Table II show a decrease in MLSL when the elevation stepping size is increased, while the FWHM is almost the same.

TABLE II
MLSL RATIO AND FWHM FOR SIMULATED AND MEASURED PSF.

Type	Simulation	Phantom
FWHM		
0.09 mm step	1.58 mm	1.77 mm
0.45 mm step	1.77 mm	1.75 mm
0.99 mm step	1.76 mm	1.74 mm
Stacked 2D data	3.39 mm	6.38 mm
MLSL		
0.09 mm step	14.64 dB	13.08 dB
0.45 mm step	14.52 dB	12.13 dB
0.99 mm step	11.98 dB	7.18 dB
Stacked 2D data	9.79 dB	1.09 dB

A phantom measurement of a single diamond PSF phantom was done at a depth of 65 mm. The amplitude of the PSF in elevation is shown in Fig. 5. The measurements show a higher average of the side-lobes compared to the simulation as well as an asymmetric side-lobe amplitude. The reason for the asymmetry is assumed to be because the scatterer is not perfectly below the center elevation position, and that the small diamond is not an ideal scatterer. The improvement in FWHM and MLSL when applying 3D SA focusing is better for the PSF phantom, but the starting point is poorer than for the simulation. The values are given in Table II.

An image of the measured PSF phantom is shown in Fig. 6. This image shows a slice in the elevation direction, where the extent of the scatterer is highly reduced and other impurities in the phantom are attenuated.

A cyst phantom was scanned with tubes at an angle from the elevation direction. Fig. 7 shows an image of the cyst with some homogeneous speckle on the left part. The cyst is almost not visible with a 40 dB dynamic range without

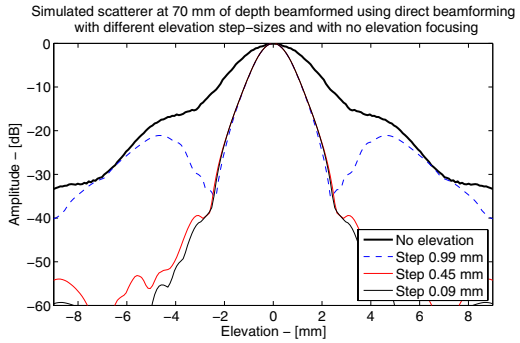

Fig. 4. Projection of the PSF of a simulated scatterer at 70 mm of depth for different elevation step sizes.

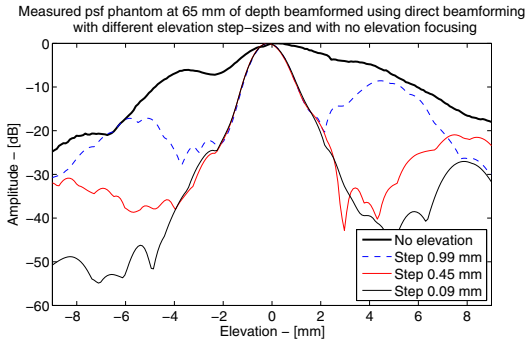

Fig. 5. Projection of the PSF measured on a PSF phantom at 65 mm of depth for different elevation step sizes.

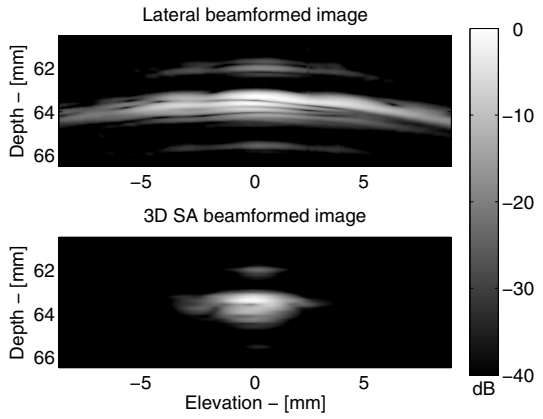

Fig. 6. PSF phantom B-mode image with and without 3D SA focusing shown in the elevation-depth plane.

elevation focusing, and shows an improvement of 5.80 dB in CNR when applying 3D SA focusing.

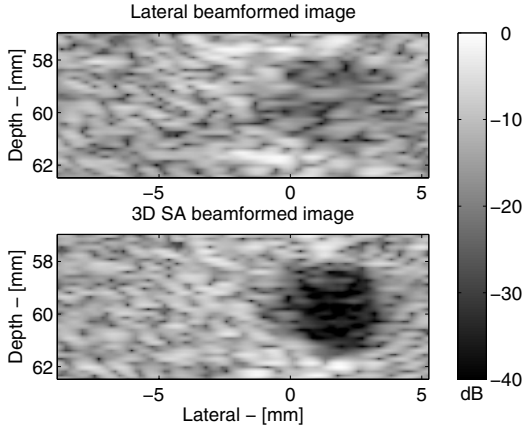

Fig. 7. B-mode image of a cyst phantom with and without synthetic elevation focusing in the lateral-depth plane. The diameter of the cyst is 4 mm.

V. Conclusion

The method shows the ability of calculating the ToF for a spherical sound wave emitted by a linear array transducer for any point within the acceptance angles of the VS defined by the transmit VS and the elevation focus VS. A bias of 0.09λ and a standard deviation of the error of 0.0049λ is found when comparing (2) to the simulated pulse-echo response of a single scatterer placed off-axis.

The method shows the ability of maintaining a constant $F^{\#}$ in the elevation direction allowing an almost constant FWHM. For a simulated scatterer at 70 mm of depth, the elevation FWHM is 3.39 mm with conventional imaging, and 1.58 mm with 3D SA focusing. The MLSL is 9.79 dB with conventional imaging, and 14.64 dB with 3D SA focusing. During a measurement on a PSF phantom containing a small diamond, the FWHM was 6.39 mm and 1.77 mm with and without 3D SA focusing, and the MLSL was 1.09 dB and 13.08 dB. The measurement showed a greater improvement then the simulations, though the starting position was poorer.

Finally the method was applied to a 3D volume scan of a cyst phantom, where the ability to improve the contrast in the conventional imaging plane was evaluated, and an improvement of 5.80 in CNR was found for a 4 mm water filled cyst.

Acknowledgment

This work was supported by grant 71122 from the Danish Ministry of Science, Technology and Innovation, grant 9700883, 9700563 and 26-04-0024 from the Danish Science Foundation and by B-K Medical, Denmark.

References

[1] C. H. Frazier and W. D. O'Brien. Synthetic aperture techniques with a virtual source element. *IEEE Trans. Ultrason., Ferroelec., Freq. Contr.*, 45:196–207, 1998.

[2] S. I. Nikolov and J. A. Jensen. 3D synthetic aperture imaging using a virtual source element in the elevation plane. In *Proc. IEEE Ultrason. Symp.*, volume 2, pages 1743–1747, 2000.

[3] S. I. Nikolov. *Synthetic aperture tissue and flow ultrasound imaging*. PhD thesis, Ørsted•DTU, Technical University of Denmark, 2800, Lyngby, Denmark, 2001.

[4] S. I. Nikolov, P. Santén, O. Bjuvsten, and J. A. Jensen. Parameter study of 3D synthetic aperture post-beamforming procedure. *Ultrasonics*, page Accepted, 2006.

[5] M. Karaman, P. C. Li, and M. O'Donnell. Synthetic aperture imaging for small scale systems. *IEEE Trans. Ultrason., Ferroelec., Freq. Contr.*, 42:429–442, 1995.

[6] S. I. Nikolov and J. A. Jensen. Virtual ultrasound sources in high-resolution ultrasound imaging. In *Proc. SPIE - Progress in biomedical optics and imaging*, volume 3, pages 395–405, 2002.

[7] F. Gran and J. A. Jensen. Designing non-linear frequency modulated signals for medical ultrasound imaging. In *Proc. IEEE Ultrason. Symp.*, page Accepted, 2006.

[8] J. A. Jensen, O. Holm, L. J. Jensen, H. Bendsen, S. I. Nikolov, B. G. Tomov, P. Munk, M. Hansen, K. Salomonsen, J. Hansen, K. Gormsen, H. M. Pedersen, and K. L. Gammelmark. Ultrasound research scanner for real-time synthetic aperture image acquisition. *IEEE Trans. Ultrason., Ferroelec., Freq. Contr.*, 52 (5):881–891, May 2005.

[9] J. A. Jensen and N. B. Svendsen. Calculation of pressure fields from arbitrarily shaped, apodized, and excited ultrasound transducers. *IEEE Trans. Ultrason., Ferroelec., Freq. Contr.*, 39:262–267, 1992.

[10] J. A. Jensen. Field: A program for simulating ultrasound systems. *Med. Biol. Eng. Comp.*, 10th Nordic-Baltic Conference on Biomedical Imaging, Vol. 4, Supplement 1, Part 1:351–353, 1996b.

[11] F. N. Ucar and Mustafa Karaman. Beam space processing for low-cost scanners. In *Proc. IEEE Ultrason. Symp.*, pages 1349–1352, 1996.